ELSEVIER

Journal of Volcanology and Geothermal Research 118 (2002) 299–317

Journal of volcanology and geothermal research

www.elsevier.com/locate/jvolgeores

Locating pyroclastic flows on Soufriere Hills Volcano, Montserrat, West Indies, using amplitude signals from high dynamic range instruments

A.D. Jolly [a,b,*], G. Thompson [b,c], G.E. Norton [b,c]

[a] *University of Leeds, Department of Earth Sciences, Leeds, LS2 9JT, UK*
[b] *Montserrat Volcano Observatory, Montserrat*
[c] *British Geological Survey, Keyworth, Nottingham, NG12 5GG, UK*

Received 9 August 2001; received in revised form 30 January 2002; accepted 30 January 2002

Abstract

Pyroclastic flows are located using amplitude signals from a seven-station high dynamic range seismograph array located 1.9–6.1 km from Soufriere Hills Volcano in Montserrat, West Indies. Locations are determined by measuring the seismograph signal amplitude for an event recorded at several stations in a moving time window analysis. For a given window, the measured amplitudes are corrected to a trial source location by removing the effect of the surface wave geometric spreading, instrument gain, and the attenuation at calculated travel-times. The trial source location is then compared to other trial locations via an iterative localised grid search where the root-mean-squared amplitude residual (δA) is minimised. The process is repeated for subsequent time steps resulting in a best-fit event location and size through time. The method has been tested on four small events occurring on April 8, 1999, August 12, 1999, February 25, 2001, and July 4, 2001, when visual observations of pyroclastic flows coincided with good seismograph station coverage (number of stations $\geqq 5$, azimuthal gap $< 160°$). Based on the location results the four events propagated ~ 0.5, 1.4, 1.3 and 1.0 km from the dome, and had maximum attenuation-corrected reduced displacements (D_{RQ}) of 9.0, 2.8, 6.9 and 2.3 cm^2 and maximum pyroclastic flow velocities of 7, 30, 20 and 8 ms^{-1}, respectively. A time-lapse video of the event of August 12, 1999, shows that amplitude-based location through time closely matches the observed run-out distance and velocity. In contrast, amplitude-based locations for the events of April 8, 1999, and July 4, 2001, underestimated the actual flow run-out by 1.5 km. Underestimation of the true run-out distance is probably due to both the increased distribution of sources as coherent dome material disaggregates into many blocks, and signal contamination from other sources. Results indicate that pyroclastic flows and rockfalls can be located using amplitude signals from high dynamic range seismograph stations yielding estimates of size and trajectory, regardless of visibility conditions on the volcano. This new method is being tested as a hazard mitigation and research tool on Montserrat.

Keywords: pyroclastic flow; amplitude-based location; attenuation-corrected reduced displacement; Montserrat

1. Introduction

Pyroclastic flows and rockfalls are comprised of hot rock and ash that propagate downslope due

* Corresponding author..
E-mail address: aj@earth.leeds.ac.uk (A.D. Jolly).

0377-0273/02/$ – see front matter © 2002 Elsevier Science B.V. All rights reserved.
PII: S0377-0273(02)00299-8

to gravity. Such events are usually associated with intermediate to silicic volcanoes and commonly occur on growing domes that can be perched at higher elevation. Some recent examples of volcanoes having periods of dome growth and failure include Unzen (Nakada et al., 1999), Redoubt (Miller and Chouet, 1994), Merapi (Voight et al., 2000), and Montserrat (Young et al., 1998). Pyroclastic flows and rockfalls from such domes are commonplace because the edifice is gravitationally unstable, loosely consolidated and actively deformed.

On the island of Montserrat in the West Indies (Fig. 1), rockfalls and pyroclastic flows originate from a dome located in a horseshoe-shaped sector collapse scar in the Soufriere Hills. The dome was extruded beginning November 1995 (Young et al., 1998), and continued through March 1998, after which dome growth ceased (Norton et al., in press). Slow extrusion and dome growth resumed in November 1999 after a 20-month quiescence (Norton et al., in press) and continues to the time of this paper (July 2001).

Repetitive failure of the dome occurred

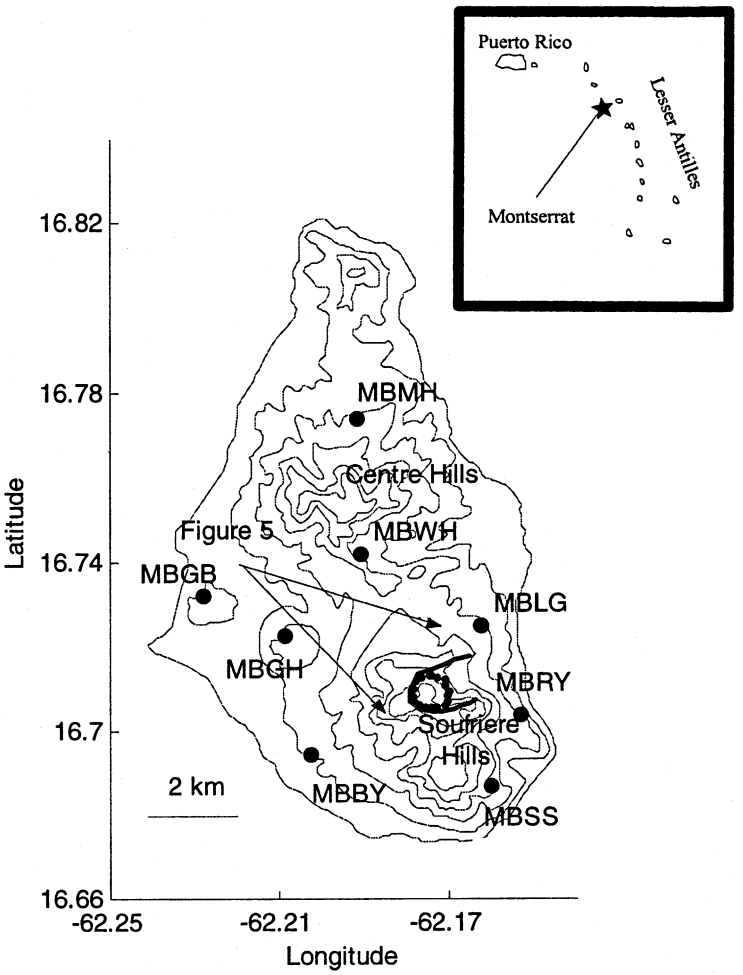

Fig. 1. Location map of Montserrat with locations of high dynamic range seismograph stations (large dots). The station MBMH was not used. Elevation contour intervals are 150 m. The arrows indicate the field of view for Fig. 5. The dome (small dots) and horseshoe-shaped collapse scar (heavy solid line) are located in Soufriere Hills. Major valleys that constrain pyroclastic flows are shown in Fig. 5.

throughout the period from 1996 to the present. The Montserrat Volcano Observatory (MVO) classifies the smaller of these events as rockfalls, while larger events are called pyroclastic flows. The latter are notorious and have resulted in loss of life on Montserrat and at other volcanoes worldwide. Thus, characterising events of these types are important from a hazard mitigation standpoint.

Some important fundamental parameters associated with the pyroclastic flow include its location, size and direction of propagation. This information is commonly obtained by direct visual observation but characterisation may be hindered by poor visibility due to low clouds, darkness or an incomplete view of the volcano. Correlation of rockfall and pyroclastic flows with seismograph recordings is commonplace, and volcano observatories often attempt to determine generalised locations based on relative amplitudes at several seismograph stations. This 'eyeball' technique is useful but inexact, and provides no information about propagation of an event through time. Furthermore, the size of the event is ill-constrained because the signal amplitude is distance dependent and poorly known. To improve on this inexact method, we have devised a pyroclastic flow location technique based on the signal amplitude at multiple seismograph stations. The method provides the location and size for each of several segments of the event, with variations in the location being dictated by variations of signal amplitudes at the available stations.

2. Theory

The character of rockfall and pyroclastic flow events is developed from both visual and seismological observation. Such events usually initiate at some point at or near the surface of the dome and then propagate gravitationally downslope. The triggers for a pyroclastic flow are numerous and might include an explosion, an extrusion, a dome intrusion or a gaseous venting (Ui et al., 1999). Such triggers might be reflected in the onset of seismicity with a rapid onset indicative of an extrusive or explosive trigger, while a slower, more emergent onset might indicate a gravitational trigger. As the event proceeds, the source area widens. Material that might initially comprise a coherent block, rapidly disaggregates into smaller blocks, which subsequently flow downslope producing ground motions detectable at surrounding seismograph stations (Uhira et al., 1994). The ground motions recorded on seismographs have ragged envelope wave-trains (Fig. 2A and C) and variable durations. Their spectra are typically broad-band but may contain a peaked low frequency (1–4 Hz) component at their onset (Fig. 2B and D). This low-frequency pulse might be associated with resonance of a bubbly fluid-filled magma system (Chouet, 1988; Neuberg et al., 2000). Overtones of this fundamental peak are often observed at higher frequencies (cf. Benoit and McNutt, 1997; Rowe et al., 2000; Neuberg et al., 2000).

The signal observed at one or more seismograph stations thus records the onset that initiates at a single location, followed by multiple moving sources that might be spread over a large area. Existence of multiple sources makes standard earthquake location methods unrealistic; the signals of any one source reside in the codas of multiple preceding sources. The amplitudes of the totality of sources are recorded, however, and these amplitude data can be exploited to determine an integrated (average) location for the event. This is possible because the signal amplitude is expected to decay with greater distance (and travel-time) from the source area according to the equation:

$$A = (1/s)A_o \exp[-\pi f t/Q] \quad (1)$$

where A is the observed amplitude at some frequency f for a given time t. The amplitude decay with time is due to two factors, the geometric spreading of waves s and the attenuation Q. Because the phenomena originate and propagate near the earth's surface, the first factor is likely to be a simple surface wave geometric spreading:

$$s = \sqrt{r}\sqrt{\lambda} \quad (2)$$

where r is the distance from the source to the station and λ is the wavelength of interest (Fehler,

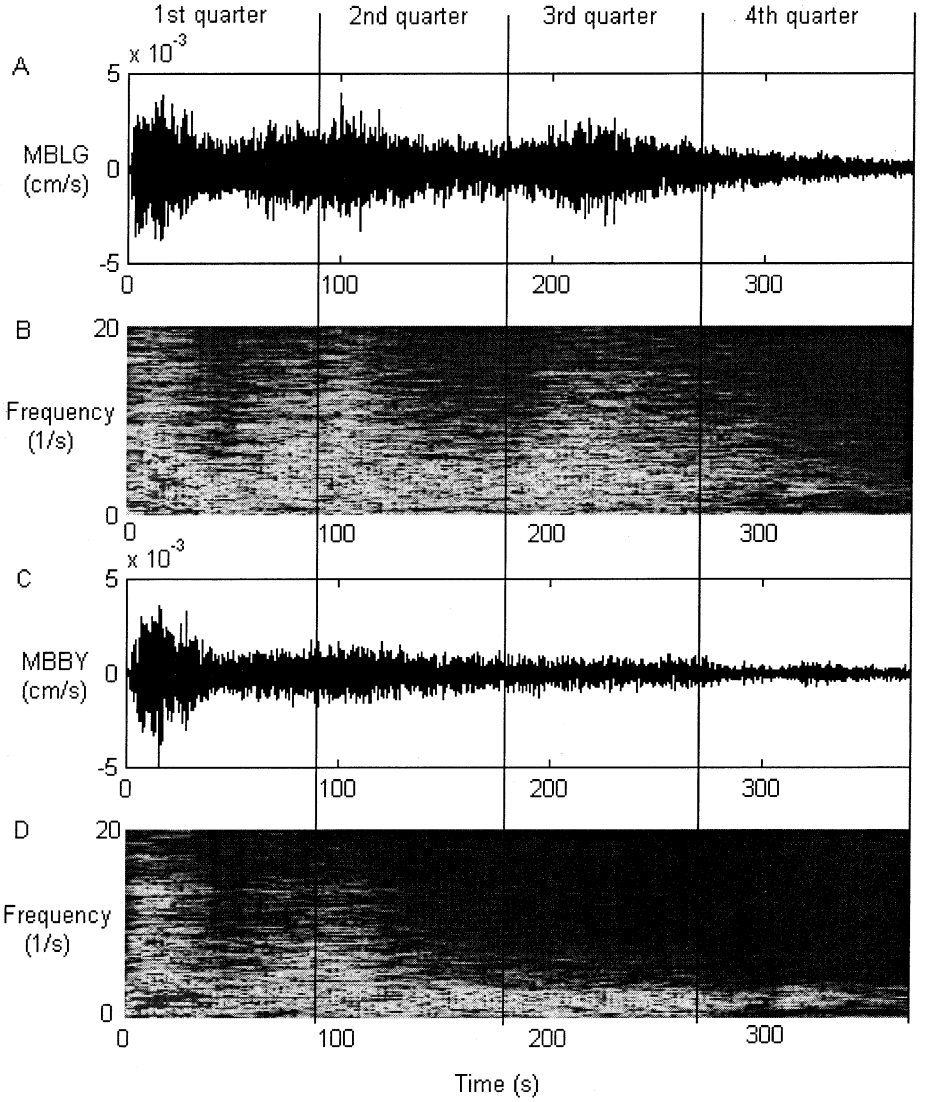

Fig. 2. Typical seismograms (A and C) and spectrograms (B and D) for an event recorded on August 12, 1999. The stations are MBLG (A and B) and MBBY (C and D), respectively (see Fig. 1). Note the second phase at the time 80–140 s on station MBLG and the third phase at 200–250 s. The strong peak at 1–4 Hz (B and D) is probably associated with the conduit resonance while later phases (pyroclastic flow) have broad-spectra energy at higher frequencies. The quarter segments for this event are shown to aid in comparison of waveforms and spectra (this figure) to associated locations (Fig. 6) and amplitude (Fig. 7).

1983). The second decay factor Q is unknown, but it can be estimated for an assumed travel-time t, allowing determination of the amplitude at the source A_o:

$$A_o = As/\exp[-\pi ft/Q]. \quad (3)$$

Finding the source location with amplitude information at several stations is straightforward; high amplitude signals indicate that the source is nearby while lower amplitude signals indicate the source is more distant. Using Eq. 3, we can find the best-fit location from amplitude measurement on many stations. Forms of this methodology have been applied to find the epicentre of tremor at Bromo Volcano located in Indonesia (Gott-

schammer and Surono, 2000), to locate rockfalls at Piton de la Fournaise (Aki and Ferrazzini, 2000) and to locate pyroclastic flows at Unzen Volcano, Japan (Yamasoto, 1997). The method is also analogous to the standard earthquake location problem (Lahr, 1989), where an earthquake's location is determined based on known arrival times in an assumed velocity structure with time related to distance via the velocity. We use similar methods here.

3. Seismograph data

The Montserrat Volcano Observatory operates an eight-station network located between 1.5 and 9.0 km from the active dome. The network includes five three-component Guralp 40T broadband seismometers and three short-period vertical component Integra LA 100's. The data are digitised in the field and transmitted to the observatory via radio where they are recorded at a sampling rate of 75 Hz. The broadband and short period instruments have a dynamic range of 145 and 100 dB and a magnification of 5.0×10^9 and 2.0×10^9, respectively, at 1 Hz.

For the period April, 1999–July 4, 2001, the network had static array geometry, and recorded extensive low-level rockfall and dome collapse activity. Several larger dome collapse events occurred including events on August 25, 1999, March 30, 2000, and July 31, 2001. Unfortunately, these events occurred during periods when the network was either not recording or recorded only on a small subset of stations. Instead we used events that were recorded on several stations of the local network and were accompanied by visual observations of pyroclastic flow activity. Events satisfying these criteria occurred on April 8, 1999, August 12, 1999, February 25, 2001, and July 4, 2001 (Table 1). All events are on scale through the entire event on all stations, a distinct advantage of high dynamic range instruments over their analogue counterparts. The latter may be off scale for large amplitude events.

4. Methods

In practice, a moving time window is applied to each station for which an amplitude signal is available. The 1024-sample (13.6 s) window is selected from vertical component seismograph velocity data and a 20% Hamming taper is applied. The amplitude spectrum is calculated for the window using a Fast-Fourier Transform (FFT) and subsequently corrected for the instrument response. Examination of moving window spectrograms for pyroclastic flows (Fig. 2) indicates that the dominant energy for such events is in the frequency range 3–12 Hz. Furthermore, the dominant conduit resonance is at 1–4 Hz while the Nyquist frequency is 37.5 Hz. To measure the signal associated with the pyroclastic flow and also minimise the effect of the conduit resonance, we selected the frequency at 7–9 Hz. In addition, the 1024 sample FFT assures that signals from stations at relevant distances are recorded faithfully. For example, two stations 6 km apart, have surface wave signals $\sim$4 s apart (assuming a surface wave velocity of 1500 ms^{-1}), well within the 13.6-s window of the FFT.

After calculating the amplitudes at all stations, they are corrected to a trial location using Eq. 3. The corrected amplitudes A_o are averaged and residuals from the mean are determined. From the residuals, the root-mean-squared (RMS) am-

Table 1
Events used in location analysis

Date (day-month-yr)	Time (UT)	Number stations	Visual observation
08-04-99	02:02 h	7	pyroclastic flow in Tar River
12-08-99	11:41	5	pyroclastic flow in Tar River
25-02-01	20:35	6	pyroclastic flow in Tuitt's Ghaut
04-07-01	21:23	6	pyroclastic flow in Gages

Table 2
Procedure chart for amplitude location algorithm

(1)	Select event onset
(2)	Calculate 1024-sample FFT for all stations and correct for instruments
(3)	Measure station amplitude at 7–9 Hz for each station
(4)	Select trial location, determine source-station distances and surface wave travel-times
(5)	Determine amplitudes at selected trial location for each station from source station distances, travel-times and assumed Q-value
(6)	Determine mean amplitude and station amplitude residuals, and RMS amplitude residuals.
(7)	Repeat steps 4–6 for neighbouring locations
(8)	Select location with the lowest RMS amplitude residual as new trial location and repeat steps 5–8 until minimum RMS amplitude residual is determined
(9)	Move time window by 256 samples and repeat steps 2–9
(10)	Stop at end of event

plitude residual (δA) is determined. The δA will vary depending on the location, with the lowest δA corresponding to the best agreement between the amplitude data from all the stations. We found the minimum δA by conducting an iterative localised grid search. The search is initiated at a central trial location and at neighbouring trial locations. The least-squared minimum among these trials is taken as the new central trial location and the process is repeated until a location having the minimum δA is found. As a compromise between computational speed and location accuracy, the method found δA for both close neighbours ($\sim$9 m from the central trial location) and far neighbours ($\sim$0.9 km). The far neighbours allowed rapid convergence towards minimum δA while the close neighbours found the minimum δA to a high computational accuracy. After the location with the minimum δA is determined, the time window is incremented by 256 samples (3.41 s) and the process is repeated (Table 2). The 256-sample time step is somewhat arbitrary but was selected to smooth the location results for each event.

The amplitude location process relies on an estimate of the attenuation Q and travel-time t at the surface. These parameters are unknown and there is a direct tradeoff between them (Eq. 1). Regardless, if the travel-time is calculated from an assumed velocity, then the 'best' Q can be determined by monitoring the RMS amplitude residual. Alternatively, Q could be assumed at a fixed value and the optimum surface wave velocity determined. Constraining these values require that the location of the event is known. To this end, we selected the onsets of three of the events of this study (April 8, 1999, August, 12, 1999, and February 25, 2001) because their location is constrained within the dome. For the fixed location and known station amplitudes, the RMS log amplitude was monitored at several trial Q values and assuming a velocity of 1500 ms^{-1}. The range of Q at the minimum RMS log amplitude is between 18 and 30 for the onsets of the three events (Fig. 3). The minimum RMS for all three events ($Q=23$; Fig. 3, dashed line) is used to locate all events. Furthermore, the individual amplitude residuals for the three event onsets were examined with respect to the mean amplitude in order to determine whether any systematic signal amplifications occurred at specific stations. These amplification factors were averaged and applied as station amplification corrections for the three events (Table 3). Our Q and station correction results are dependent on the assumption that the events did initiate within the dome. We believe this is a sound assumption because the dome is unstable, steep and is being actively deformed. In addition, visual observation since 1995 has shown that rockfalls and pyroclastic flows concentrate at the dome and not elsewhere on the volcano.

The Q estimation technique was further tested using synthetically determined amplitudes for a source at the summit having $Q=23$ and a surface velocity of 1500 ms^{-1}. Then, in several trials, we searched for the minimum Q for a fixed source within $\sim$400 m from the synthetic source (about the maximum lateral extent from the centre to the

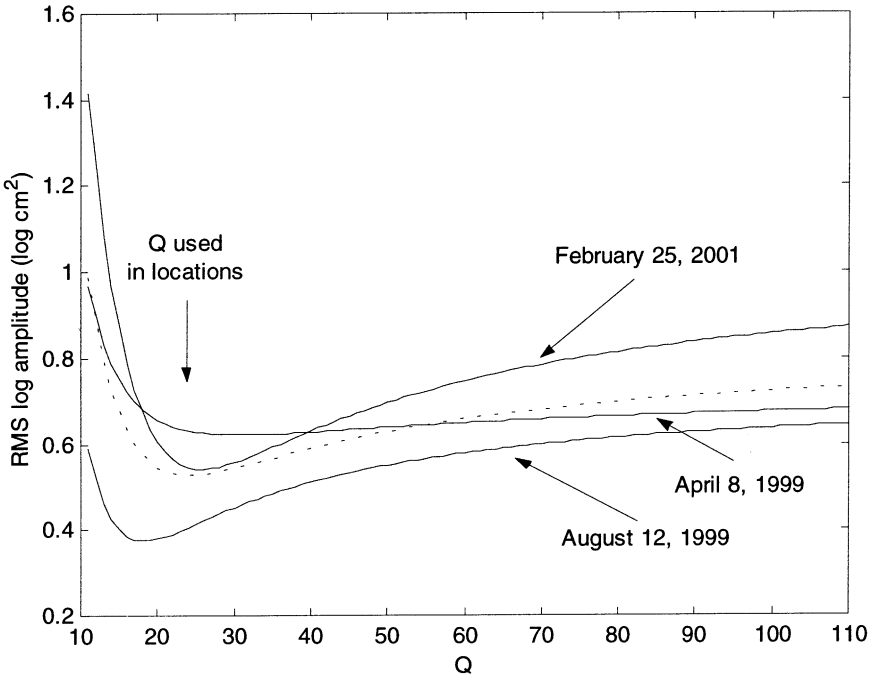

Fig. 3. The RMS log amplitude at several trial Q values for the onset of three events used in this study. The Q values are calculated assuming the source was fixed at the dome. The residuals are calculated from the average of the logs of all available stations. The April 8, 1999, and August 12, 1999, events have a minimum RMS at $Q=30$ and $Q=18$, while the February 25, 2001, event has a minimum amplitude at $Q=25$. The mean Q for all three events is shown in the dashed line and has minimum $Q=23$ which is used for the location of all events.

edge of the dome) and having a velocity of 1500 ms^{-1}. In these trials Q ranged by ± 3 of the actual (synthetic) value.

Because the surface wave velocity is unknown, the actual attenuation value is not constrained. If we selected a slower surface wave velocity, the 'best' agreement in amplitude data would require a weaker attenuation value. This assertion was confirmed by assuming an alternative surface wave velocity of 900 ms^{-1}, finding the minimum RMS log amplitude residual (at $Q=30$) and then relocating the events. We found that the location matched closely (within 200 m) the value determined using 1500 ms^{-1} and $Q=23$ but that the amplitude was about 25% higher. This is because the surface wave geometric spreading correction (Eq. 2) depends on the wavelength λ. We discuss these errors in the amplitude and location method below (see 6.1. Error and accuracy estimates.

The amplitude-based location method is applied to four events (Table 1) that are well recorded on the Montserrat broadband network. The located events have coincident visual observations and thus are ideal for testing the method.

Table 3
Amplification factors at 7–9 Hz for the onsets of three events used in this study

Station	MBRY	MBSS	MBBY	MBGH	MBGB	MBWH	MBLG
Event							
08-04-99	0.252	1.165	1.439	0.970	2.036	0.451	0.683
12-08-99	0.501	1.125	0.869			0.774	1.728
25-02-01	0.434	0.803		0.801	1.768	0.859	1.332
Correction	0.396	1.031	1.155	0.886	1.903	0.696	1.249

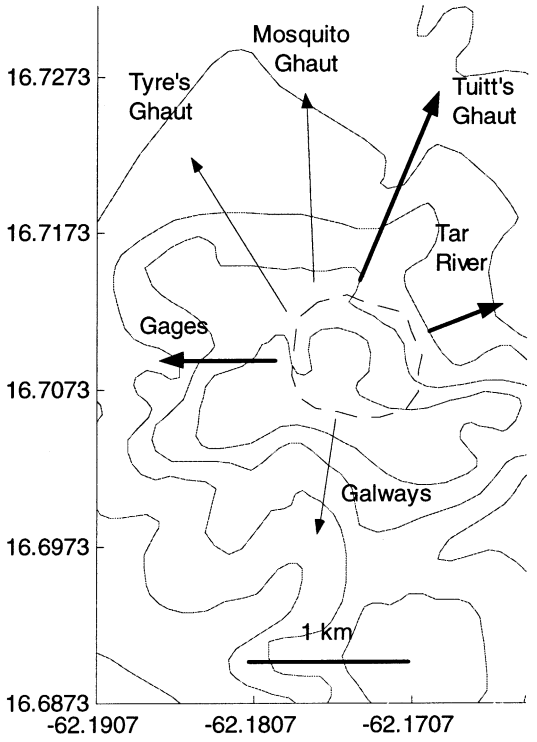

Fig. 4. Typical directions for pyroclastic flows at Montserrat. The events in this study propagated down the Tar River Valley, Tuitt's Ghaut and Gages (bold arrows) (Table 3).

In each case, the amplitude-derived locations matched closely the visual observations. Useful parameters derived from the method include the best-fit location for the event through time (onset location and trajectory), the amplitude of the signal at its best-fit location and the flow velocity. We scale the amplitude to the reduced displacement (Aki and Koyanagi, 1981; Fehler, 1983), giving a new attenuation-corrected amplitude measurement

$$D_{RQ} = A_o/2\sqrt{2} \tag{4}$$

here called the attenuation-corrected reduced displacement, a measure of event amplitude equal to ground displacement corrected for the geometrical spreading (Eq. 2) and the attenuation (this study; Eq. 3). This parameter has the same units (cm^2) as the classical reduced displacement. It is noted for comparative purposes that attenuation-corrected reduced displacements are larger than their non-attenuation-corrected counterparts. In this study, the attenuation-corrected reduced displacements are about an order of magnitude larger than the uncorrected reduced displacements.

Fig. 5. Photo showing the February 25, 2001, pyroclastic flow propagating from the dome into Tuitt's Ghaut. The photo was taken from Old Towne viewing southeast (see Fig. 1). Photo courtesy Paul and Elizabeth Breuer.

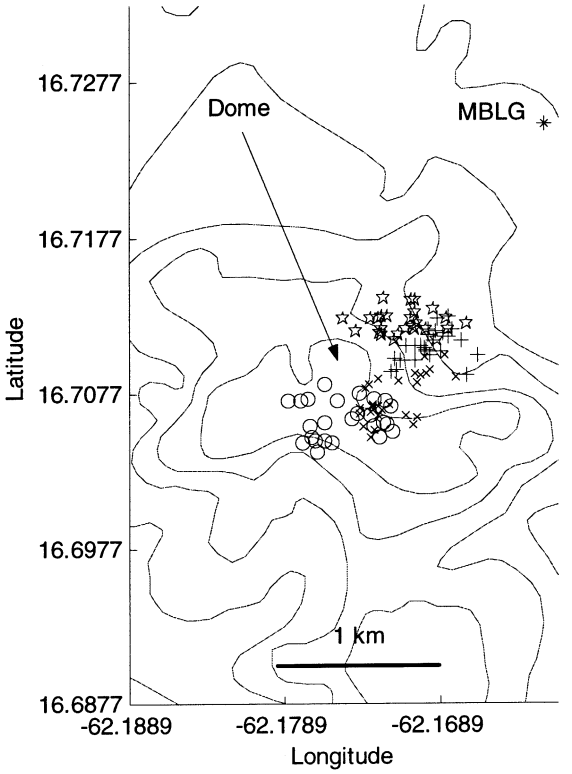

Fig. 6. Amplitude-based locations for the event recorded on April 8, 1999. The event is divided into four time intervals to show event location through time. The first time quarter is designated by circles, the second by crosses, the third by plus signs, and the fourth by stars. The amplitude-based locations suggest that the event initiated on the southern part of the dome and subsequently propagated down the Tar River Valley.

5. Pyroclastic flow data and results

The MVO has observed thousands of pyroclastic flows and rockfalls in all azimuthal directions (Fig. 4) over the period of the eruption. Only a small number of events, however, have good visual observations coincident with a fully functional broadband network. The selected events (Table 1) were located at Soufriere Hills Volcano on seven of the eight seismographs located between 1.9 and 6.1 km from the dome (Fig. 1). The event occurring on April 8, 1999, was documented in a visual observation log (Norton et al., in press; Table 1) that contains basic information including its time of origin, general location and direction of propagation. The second event, occurring on August 12, 1999, was recorded on the MVO time-lapse video camera located in the Centre Hills (Fig. 1). The February 25, 2001, event was observed by two of the authors (A.D.J. and G.E.N.), and also was independently photographed (Fig. 5). The fourth event, occurring July 4, 2001, was added to demonstrate that the method is capable of locating events at alternative azimuthal directions from the dome. Together, the example events provide strong support for the amplitude-based location method as a hazard mitigation and research tool.

5.1. The April 8, 1999, event

The April 8, 1999, event was noted as a small pyroclastic flow that propagated down the Tar River Valley (Fig. 4). The event was recorded on seven of the eight available stations (MBRY, MBSS, MBBY, MBGH, MBGB, MBWH, and MBLG), providing strong constraints for both the final location and amplitude. The event had three distinct phases at MBLG (Fig. 2A), but the second and third phases were only weakly observed on station MBBY (Fig. 2C). The second phase was also observed on stations MBRY, MBWH and MBSS (not shown) located east of the dome, and was weakest to the west. The location of the event (Fig. 6) and associated time amplitude function (Fig. 7) suggest that the first phase is probably the initiation of the event near the southern part of the dome (circles in Figs. 6 and 7), while the second phase records a pyroclastic flow located in the Tar River Valley (crosses and plus signs in Figs. 6 and 7). It is surmised that the event could not flow southward from its initiation point because it encountered the southern wall of the sector collapse scar (Fig. 1). The high amplitude second phase might be due to the impact between the pyroclastic flow and the relatively flat lowlands below the volcanic edifice. This effect was observed for many rockfall events by MVO scientists who correlated strong amplitude signals to the break in slope by monitoring audible modulations from a voltage-controlled oscillator at a short-period seismometer (J. Neuberg, personal communication).

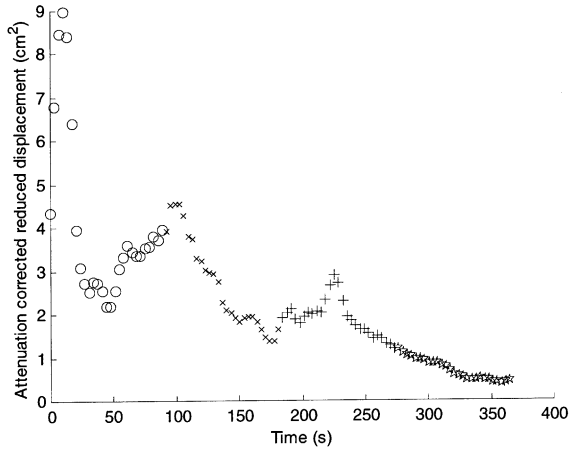

Fig. 7. Mean attenuation-corrected reduced displacement for the April 8, 1999, event at the best-fit location (see Fig. 6). Symbols are identical to those in Fig. 6.

The measured amplitude for the initial event is $D_{RQ} = 9.0$ cm^2 while the highest amplitude for the second pulse is $D_{RQ} = 4.5$ cm^2 (Fig. 7). From the amplitude-based location, the event only propagated about 500 m and had a velocity of 3–7 ms^{-1}. MVO's visual observation log reported that new deposits from this event were seen within 20 m of the shore (~2000 m from the dome). For this event the location programme underestimated the total run-out by ~1500 m. This underestimation probably indicates that some events contain more complicated time histories. The underestimation might occur because the source energy is spread over a larger area for some events. Alternatively, the event wave-trains might contain energy from multiple rock failures at the dome which dwarf the deposition energy in the body and head of the pyroclastic flow. The method will measure the integrated average of the totality of these energy sources suggesting that the location should always underestimate the total run-out of the pyroclastic flow.

5.2. The August 12, 1999, event

The August 12, 1999, event was recorded on MVO's time-lapse video camera system located in the Centre Hills (Fig. 1). The camera recorded a ~7-min event that originated at the dome, and subsequently propagated down the Tar River Valley (Fig. 8). The video footage shows that the event propagated as far as the village of Long Ground (station MBLG in Fig. 1) located about 1.9 km from the dome. The pyroclastic flow emerges from a cloud layer that obscures the onset of the ash flow, although the time elapsed and total distance of propagation are well determined (Fig. 8, positions a–g). Based on the video, the flow propagated ~700 m in the first 75 s (~9 ms^{-1}) (Fig. 8, positions a–d) and then traveled an additional 800 m in the next 40 s (~20 ms^{-1}) (Fig. 8, positions e–f). The remaining portion of the event produced abundant ash but little additional flow run-out (~200 m) on the video (Fig. 8, position g). The total observed run-out distance for this event is ~1500 m, not including run-out within the cloud-obscured dome. The distances and velocities are only approximate because they are estimated off angle and are obscured by local topographic ridges. Regardless, the event's location-time history is available for comparison to the seismological observations that recorded the event on five operating seismic stations (MBRY, MBSS, MBBY, MBWH, and MBLG). From

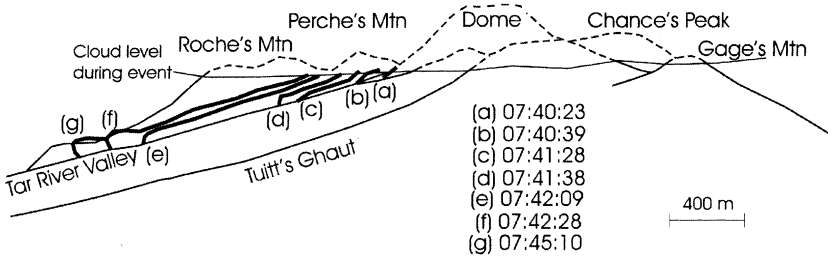

Fig. 8. Schematic diagram extracted from video footage recorded on August 12, 1999, showing pyroclastic flow location through time. The view of the video camera is to the south from the Centre Hills (Fig. 1). Times are approximate local time (without GPS timing).

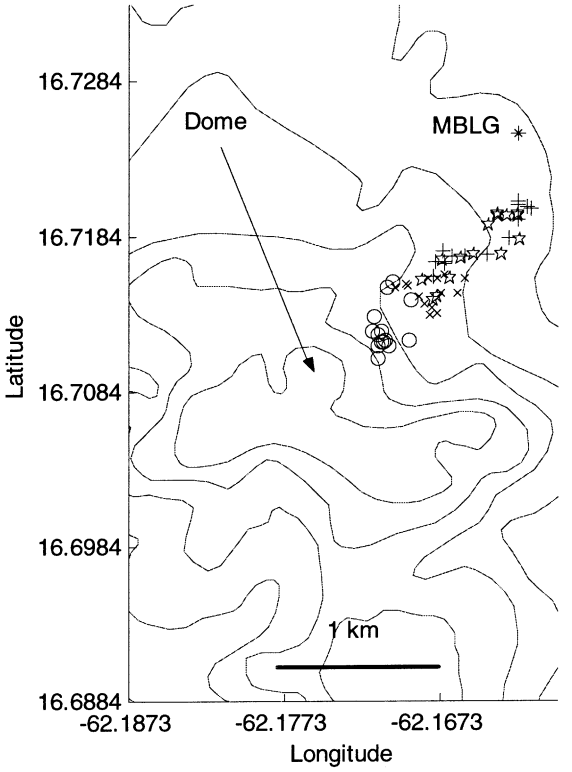

Fig. 9. Amplitude-based locations for event recorded on August 12, 1999. Symbols are identical to those in Fig. 6. The event propagated down the Tar River Valley.

these signal amplitudes, the event's onset is determined to be at the eastern portion of the dome (Fig. 9) while later stages of the event propagated eastward consistent with the time-lapse video (Fig. 8). The amplitude for the initial event is D_{RQ} of 2.8 cm^2 while the highest amplitude for a secondary phase is $D_{RQ} = 1.5$ cm^2 (Fig. 10). Spectral analysis of stations located away (Fig. 11A) and towards the direction of propagation (Fig. 11B and C) show the low frequency conduit resonance at the onset of the event (first phase) and the broadband signal (phases 2 and 3) associated with the propagation down the Tar River Valley (Fig. 11B and C). Run-out distances and velocities obtained from the amplitude-based locations indicate that the event initiated ~300 m east of centre of the dome and propagated a total distance of about 1400 m (Fig. 11D, solid line). Dome failure propagated very slowly at first, as indicated by the strong amplitude signals and low initial offset, but then propagated ~600 m in ~90 s (~7 ms^{-1}) a period coincident with the second phase observed on the seismograph array (MBLG, MBRY and MBSS) (Fig. 11B and C). The signal amplitude subsequently decreased at stations MBRY and MBSS but remained anomalously high at station MBLG (Fig. 11A–C). This third phase coincided with a rapid increase in pyroclastic flow velocity as the event propagated an additional ~600 m in ~20 s (~30 ms^{-1}). For the final 60 s of the event, the amplitude-based location appears to recede back upslope by ~500 m, coincident with low amplitude signals on all seismographs.

The video footage and amplitude-based locations appear to coincide very well for the August 12, 1999, event. The displacements and velocities for the video footage are in local time and have no external time stamp. However, the point where the pyroclastic flow emerges from the clouds is known (about 400 m east of the dome summit) and is matched to the point where the amplitude-based location was also 400 m east of the summit (Fig. 11D, first diamond). Subsequent measurements of the pyroclastic flow's location with respect to time are then determined with respect to the fixed time and distance (Fig. 11D, diamonds). The close correlation between video-measured distances and amplitude-based locations is exceptional (Fig. 11D, solid line versus diamonds and

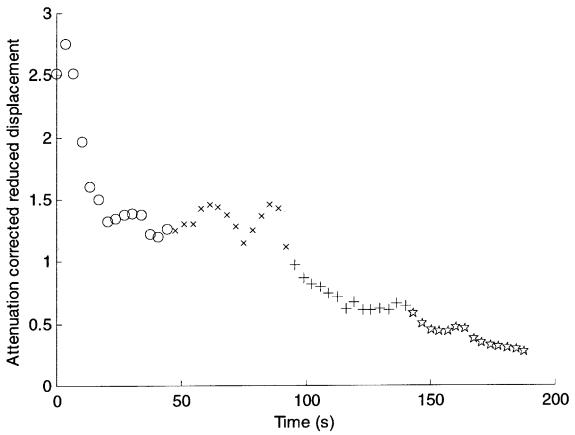

Fig. 10. Mean attenuation-corrected reduced displacement for the August 12, 1999, event. Symbols are identical to those in Fig. 6.

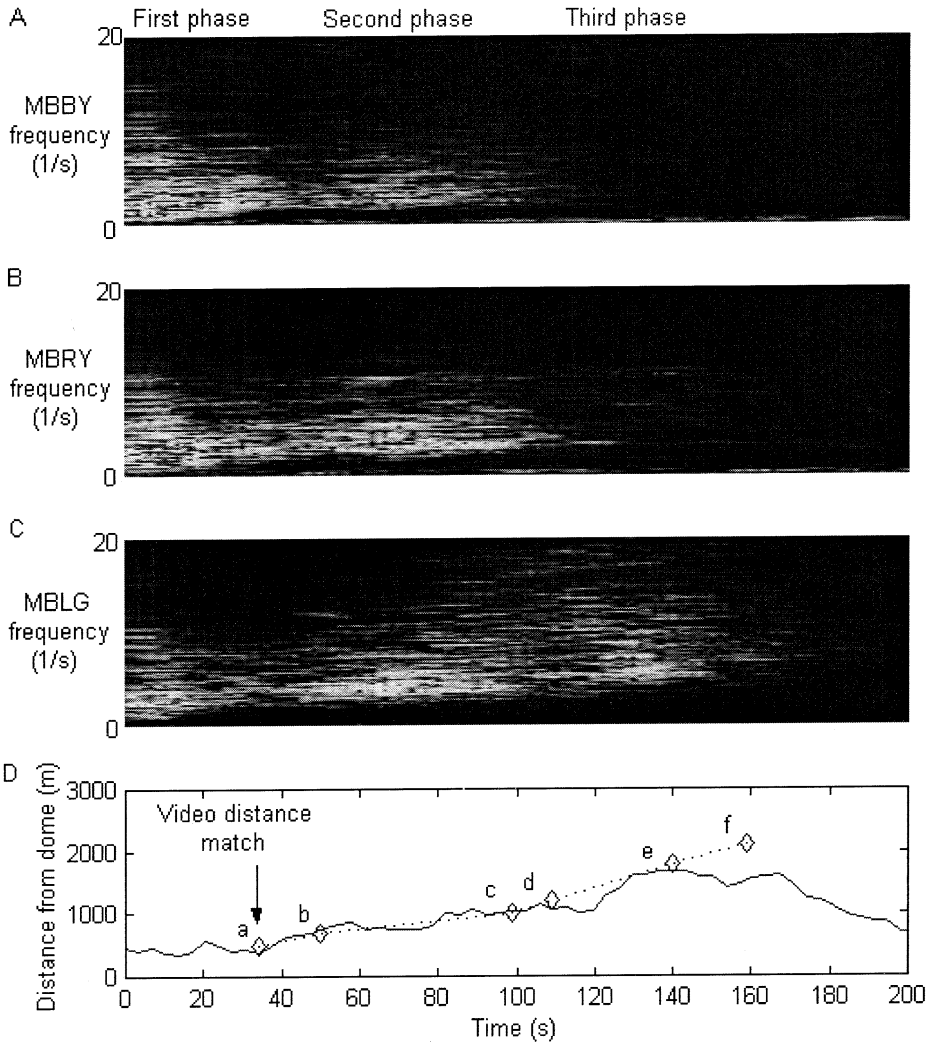

Fig. 11. Spectrograms for stations (A) MBBY, (B) MBRY and (C) MBLG reveal the onset of the pyroclastic flow during the first 20 s and the secondary phase (50 s after the onset of the event). Note the third phase at station MBLG (C). The bottom panel (D) shows the events distance from the dome with passing time for the amplitude-based location (solid line) and on the video footage (see Fig. 8)(diamonds with dashed line and letters). The video is in local time and not coordinated with external GPS. Video location is matched with the amplitude-based location at a point 400 m from the dome centre at a time 38 s after the event onset (local time 07:40:23 h on Fig. 8). Note the strong coincidence between video- and amplitude-based location. Also note the apparent back propagation (negative slope in solid line in panel (D)). Point g from Fig. 8 is not plotted for scaling reasons.

dashed line) and indicates that the amplitude-based locations closely match the visual observations in this case.

5.3. The February 25, 2001, event

The February 25, 2001, event was observed by two of the authors (A.D.J. and G.E.N.) as a pyroclastic flow propagating to the east as far as the abandoned village of Long Ground. The event was independently photographed from Old Towne (photo view in Fig. 1) that indicated a pyroclastic flow propagating down Tuitt's Ghaut (Figs. 4 and 5). This observation matches closely

the amplitude-based location (Figs. 12 and 13) derived from stations MBRY, MBSS, MBGH, MBGB, MBWH, and MBLG. The event propagates north–north–east down Tuitt's Ghaut (Figs. 12 and 13, circles and crosses) while the later stages of the event receded uphill by about 400 m in a manner similar to the August 12, 1999, event. The maximum amplitude of the event is $D_{RQ} = 6.9$ cm^2 while the secondary phase has $D_{RQ} = 3.5$ cm^2 (Fig. 13). The velocity of the flow (from the amplitude-based location) ranged between ~4–20 ms^{-1}.

5.4. The July 4, 2001, event

On July 4, 2001, a series of small events occurred on the western portion of the dome. Two of these events were observed from Garibaldi Hill (at station MBGB in Fig. 1) as small pyroclastic flows in the Gages area (Fig. 4). MVO scientists noted that the flow deposits were weathered (probably 1996–1998 dome material) and that they were deposited about 2.5 km due west from the dome. The amplitude-based locations for the two events initiated on the western part of the dome, and propagated westward consistent with observations. The events were similar in character and used the same seismograph stations (MBLG, MBRY, MBSS, MBGH, MBGB, and MBWH), hence only the latter is shown (Figs. 14 and 15). For this event, the amplitude-based location propagated about 1 km westward, and had a maximum D_{RQ} of 2.3 cm^2. Amplitude-based flow velocities for this event were between 5 to 8 ms^{-1}.

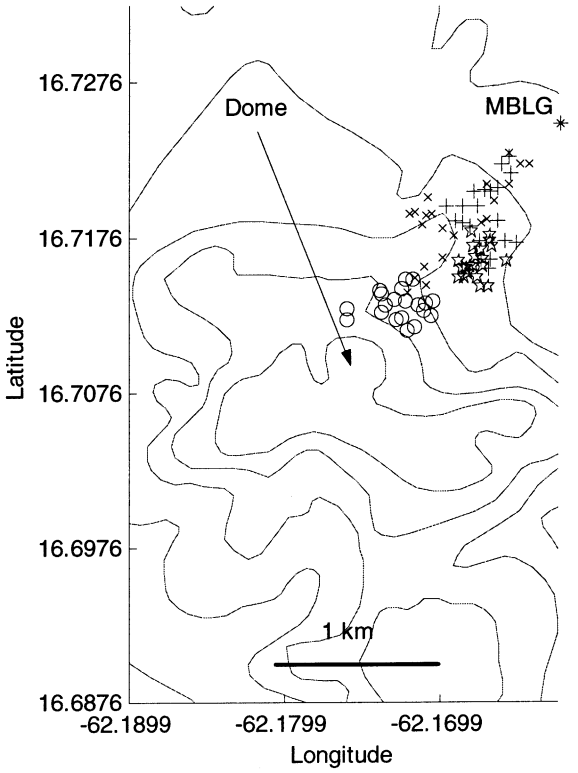

Fig. 12. Amplitude-based location for event recorded on February 25, 2001. Symbols are identical to those in Fig. 6. The event initiated on the dome and propagated down Tuitt's Ghaut (Fig. 4).

6. Discussion

The method successfully located the onsets of four events at the dome and their direction of propagation off the dome. In two cases (August 12, 1999, and February 25, 2001), the run-out distances appear to be in line with the visual observations. For the other two cases (April 8, 1999, and July 4, 2001), the method seems to underrepresent the total run-out and the velocity. Regardless, the method is successful despite several required assumptions including geometric spreading correction, seismic velocity of surface waves, and the attenuation. Such assumptions can introduce errors that affect the location and final amplitude of the event. Other factors including site resonance, velocity-amplitude coupling, changing station geometries (non-uniform phase sets), unmodeled Q, and contamination of the location by conduit resonance and the influx of other waves (body waves, reflected waves and scattered wave) can introduce additional errors. These errors are discussed and, where possible, assessed in order to provide a stronger grounding for the amplitude-based location method.

6.1. Error and accuracy estimates

For the new location method, the number of stations available for the actual measurement dic-

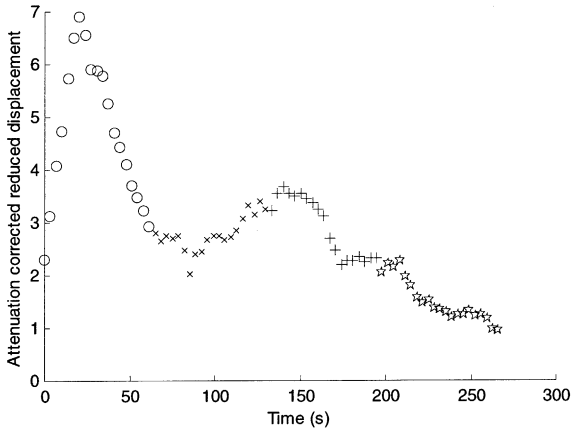

Fig. 13. Mean attenuation-corrected reduced displacement for the February 25, 2001, event. Symbols are identical to those in Fig. 6.

tates the location precision. The instruments and method used to measure the phenomena often directly affect the location precision, and using different instruments in different locations is known to strongly degrade the precision of measurements. This problem is critical in standard earthquake locations, and non-uniform phase sets (using different stations for each located earthquake) commonly reduce the precision of the locations. This limitation is relevant to the amplitude-based location method, too, but the effect is significantly reduced with high dynamic range instruments where uniform station sets are available for individual events. In this case, changes observed in the location are directly related to the amplitude relationships for the network and the relative location precision is potentially very high.

To assess the effect of changing station geometries on the amplitude-based location, the event occurring April 8, 1999, was relocated without station MBLG (Fig. 16). The relocated event is shifted by only ~200 m from the location using all seven stations (Fig. 7) and has the same general propagation direction (to the east). The event's location is observed to shift by a larger amount (analysis not shown) for locations without station corrections (Table 3). It is noted that further reducing the station number to four stations produces generally poor event locations (particularly when the relocation coincided with a large azimuthal gap). Note also that a station located in the direction of propagation is critically important. If station MBLG (Fig. 1) were unavailable, then a pyroclastic flow propagating down Tar River Valley and Tuitt's Ghaut would not be located with the same accuracy. The experiment reveals that station corrections, uniform phase sets, high station density and small azimuthal gaps are critical for accurate amplitude-based locations.

The final location and amplitude is also dependent on the Q-value used, and location and amplitude errors might result from variations from the actual attenuation. Since the attenuation at Montserrat has not been estimated, we examined the variation of Q at other volcanoes. For example, at the Katmai volcanoes, $1/Q$ varies by ~25% of the mean along the volcanic axis (Jolly,

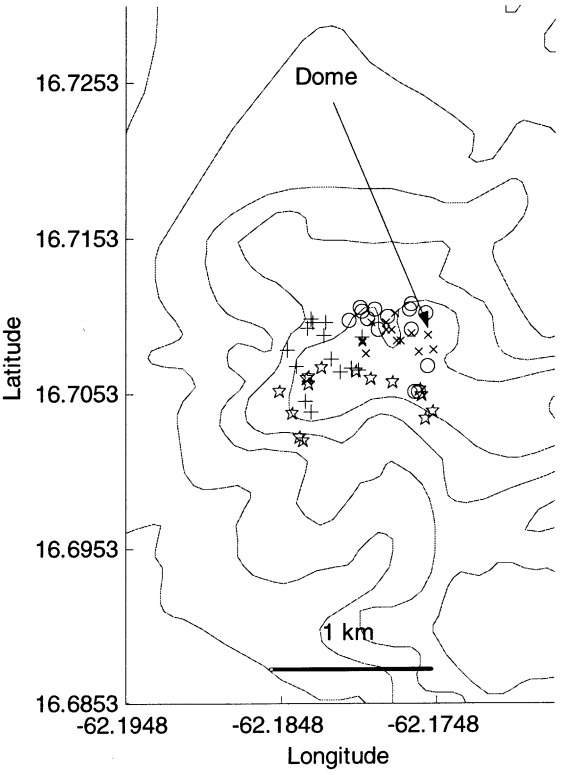

Fig. 14. Amplitude-based location for event recorded on July 4, 2001. Symbols are identical to those in Fig. 6. The event initiated at the dome and propagated down Gage (see Fig. 4).

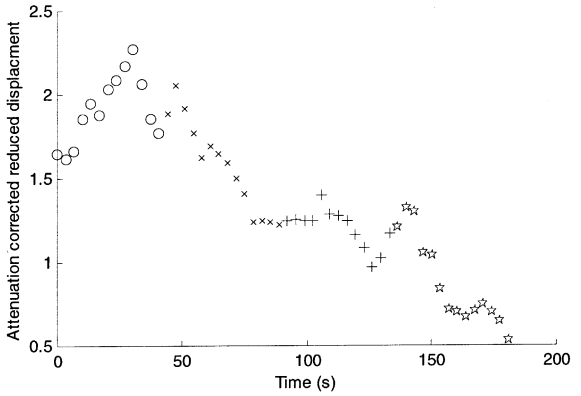

Fig. 15. Mean attenuation-corrected reduced displacement for the July 4, 2001, event. Symbols are identical to those in Fig. 6.

2000), at Newberry Caldera (Zucca and Evans, 1992) by ~10%, and at Coso (Wu and Lees, 1996) by ~40%. The Q variations are derived from inversions, and hence are strongly influenced by damping. Regardless, if $1/Q$ varies by about 10% on Montserrat, i.e. $1/Q = 0.043 \pm 0.005$, then relocations using $21 < Q < 26$ offer a rough estimate of the minimum variations due to Q. Relocation using these alternative Q values yields errors of approximately ±200 m near the dome and about ±300 m toward the edge of the seismograph array. Different attenuation values also affect the amplitude of the event. For the August 12, 1999, event, the stronger attenuation $Q = 21.0$ yielded a maximum $D_{RQ} = 3.7$ cm^2 while the relocation at $Q = 26$ yielded $D_{RQ} = 2.2$ cm^2. These errors are of about the order as errors associated with the selection of the minimum Q at an arbitrary travel-time velocity (Fig. 3) and also the errors due to the estimation of Q at an assumed location at the summit (see 4. Methods). Larger errors towards the edge of the array are due to asymmetries in the array similar to the errors associated with the earthquake location process.

The absolute accuracy is estimated by comparing the amplitude-based location to the actual location from visual observation. Strong coincidence between amplitude locations and visual observations for the August 12, 1999, event and the February 25, 2001, events suggest that the absolute accuracy is very high. The onset of all amplitude-based locations is within the dome, suggesting an accuracy of better than ~400 m. Because the later portions of the event measure multiple sources from disaggregated dome material, the actual location is more widely distributed and the average location from the integrated sources will not correspond to the leading edge of the pyroclastic flow. Thus it is difficult to gauge the absolute accuracy of the amplitude-based location against the observed run-out and velocity of the pyroclastic flow. For the August 12, 1999, event, the observed maximum run-out distance is within ~200 m of the run-out distance based on the signal amplitudes. For the April 8, 1999, and the July 4, 2001, events, the discrepancy between the observed deposits and the amplitude-based locations is much greater (~1.4 km). However, note that we make no assumption about a point source location (see 2. Theory), instead the method determines an integrated (averaged) location of all energy sources. Thus the discrepancy might indicate either that the bulk of material was deposited well upslope of the leading edge of the flow deposit or that the amplitude signal was contaminated by other sources. These possibilities are discussed below (see 6.2. Other sources of error and 6.3. Pyroclastic flows.

6.2. Other sources of error

Site resonance occurs when shallow low velocity layers trap elastic wave energy at the surface of the earth. Such wave energy is internally reflected, producing slowly decaying wave amplitudes near the seismic station. This effect might also occur in a magma conduit that resonates due to some excitation, such as an explosion. If the conduit radiates energy anisotropically, then higher amplitudes might occur on some stations preferentially. Thus conduit and site resonance might produce anomalous location results leading to a systematic mislocation. An additional problem exists because the trapped waves are produced by a strong impedance contrast. The amplitude is known to vary inversely as the square root of the impedance. Hence, lower velocities yield higher signal amplitudes. Mitigating these effects is difficult, however, examination of the site amplification at relevant

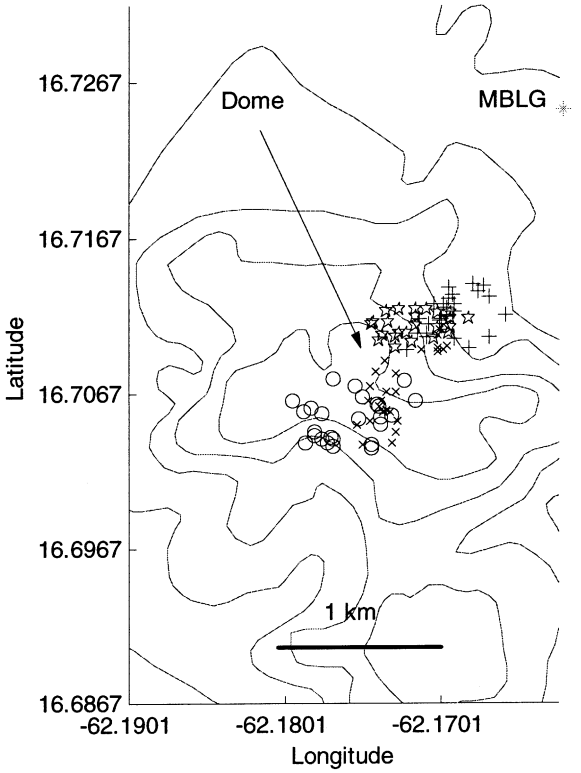

Fig. 16. Relocation of the April 8, 1999, event without station MBLG. Note the difference in locations compared to Fig. 7.

stations was conducted at the frequency of interest (7–9 Hz; Table 3) in an effort to minimise potential site amplification effects. The conduit resonance is also difficult to mitigate but here we try to minimise its effect by selecting the amplitude above the commonly observed conduit frequency (1–4 Hz) at Montserrat.

Our discussion of the conduit resonance highlights an important limitation for amplitude-based locations. Because the method measures the signal amplitudes, other energy sources may contaminate or completely mask the signal associated with the pyroclastic flow. For example, the occurrence of multiple explosive events at the dome might dwarf the signal associated with the pyroclastic flow. This effect could account for a wide discrepancy between the observed flow deposits and amplitude-based locations. However, this probably is not the case with the event on April 8, 1999, because the third phase, observed for the August 12, 1999, event (Fig. 11, MBLG) had a signal amplitude as large as its second phase indicating a high signal to noise ratio. Signal contamination might also occur if two or more pyroclastic flows occur simultaneously down different flanks of the volcano. Such a complex event could not be located successfully because the source areas are scattered over a wide area. However, important information regarding the time versus amplitude function would still be obtained. Another potential source of error might occur as a result from backscattering within the wave-train later in the event. Such backscattering is difficult to assess and might be an important source of errors. However, such contamination might be dwarfed in cases where the pyroclastic flow is sufficiently close to seismograph stations like the examples for August 12, 1999, and February 25, 2001. In summary, the amplitude-based location method works best for isolated pyroclastic flows that are not contaminated by other seismic sources.

6.3. Pyroclastic flows

The new method successfully located the onsets and propagation direction of four well-recorded events having associated visual observations. From the seismological results the events propagated between 0.5 and 1.3 km, had maximum D_{RQ} of 2.3–9.0 cm^2 and flow velocities of 3–30 ms^{-1}.

The values for the attenuation-corrected reduced displacement D_{RQ} are similar to reduced displacement values for small explosive events on volcanoes (VEI$\leq$1) (McNutt et al., 1995), but the new method represents a significant improvement over standard calculations because its results are derived from more precise locations and are corrected for the attenuation.

The run-out distances and velocities are similar to measurements of pyroclastic flow events on Montserrat determined by visual observation (Calder et al., 1999). The new location method should underestimate run-out distances and velocities for pyroclastic flows because visual methods measure the run-out distance and velocity of the fastest and furthest propagating rocks in the py-

roclastic flow front while the amplitude-based method estimates the average group velocity and average run-out distance of all of the dome material. For the April 8, 1999, event and the July 4, 2001, event, the maximum run-out distance was underestimated by about 1400 m. This discrepancy is probably due to the flow material being widely dispersed within the flow and not by signal contamination associated with near summit explosions. For the August 12, 1999, event, the maximum run-out distance based on the amplitude data was ~1400 m and the maximum distance of the pyroclastic flow based on the video data was ~1700 m (Fig. 11D). For this event, close correspondence between the observed run-out distance and flow velocity and the amplitude-based locations indicated that the flow material moved mostly at the head of the flow. Assuming that the material moved downslope as a symmetrical wave, then the bulk of the flow material was concentrated within a 400-m band at the head of the pyroclastic flow. This result corresponds closely with observations at Unzen Volcano (Yamasoto, 1997) using similar location techniques in conjunction with video observations. Observations for the four events also indicate that the latest stages of the events actually propagate back upslope towards the dome (Fig. 11D). This observation is probably not associated with a real material back propagation effect, but instead indicates that late-event energy is widely distributed within the flow. If so, then the apparent back propagation might be caused either by localised backfilling of the newly excavated dome scar or precipitation of ash cloud material at the head of the flow followed by later portions of the flow upslope. The latter might occur because leading edge flow deposits lose energy more rapidly than deposits entrained within the body of the pyroclastic flow. Either phenomenon would be masked by the event's ash cloud and could not be visually confirmed. Results from the August 12, 1999, event indicate that the velocity increased rapidly after the secondary phase diminished on stations MBRY and MBSS (Fig. 11D). The increase is also observed in the video; hence it is probably a real phenomenon. Correspondence of observations with the secondary phase (Fig. 11) indicates that the break in slope is somehow associated with the change in velocity. It is surmised that the break in slope may mark the boundary between the broadly open volcanic edifice and the incised Tar River Valley below. If so, the velocity increase might occur as a result of the flow becoming channeled in the valley, concentrating the flow energy downslope.

7. Future studies

Several future applications for the location method are envisioned. Firstly, the method is being tested as a monitoring tool. For example, the direction of rockfall and pyroclastic flow activity is strongly dependent on the area of dome growth. Hence, the locations of such activity might mark the onset of activity on a new portion of the dome. The MVO is critically interested in identifying pyroclastic flows down the Tyres and Gages areas (Fig. 3) because they are 'pyroclastic flow highways' towards the inhabited areas to the northwest of the volcano. The new location method is capable of measuring such directional changes, regardless of visibility on the dome; hence, it improves the MVO's monitoring capabilities. Secondly, the method might be applied as a forecasting tool because small-scale rockfall activity could herald the onset of larger collapses. The mechanisms for such dome instability, i.e. earthquake activity, extrusion, or gravitational over-steeping, might also be tested. If events initiate only on over-steep portions of the dome, for example, a gravitational or endogenous growth mechanism might be invoked. Alternatively, highly concentrated location at a point of known dome growth might indicate the importance of exogenous growth. Thirdly, spatial frequency-magnitude studies as applied to earthquakes (Wiemer and McNutt, 1997; Power et al., 1998) could also be applied to determine both the scaling relation of dome collapse events and regions of the dome with greater dome failure susceptibility. Zones of the dome having a strong gradient in the number of small amplitude events to large amplitude events might have an inherently lower risk for catastrophic failure compared to regions

with lower frequency-size distributions. Fourthly, the method could be used to develop improved models for pyroclastic flow dynamics, providing improved constraints on velocity, run-out distance and event size for rockfalls, pyroclastic flows and possibly surges. Finally, the method might be utilised for locations of other dispersed source phenomena such as avalanches or lahars and may be applied to the study of subsurface tremor sources.

8. Conclusions

Amplitude-based locations are determined for the first time at Soufriere Hills Volcano using a seven-station broad-band seismic network. The method provides locations accurate to within 400 m for the onset of the events, compared to visual observations with lower accuracy during later stages of the events. The final amplitudes are given in units of reduced displacement D_{RQ} corrected for both the best-fit location and the attenuation and are an improvement over fixed location estimates of the reduced displacement that do not correct for the attenuation. The method is presently being tested as a monitoring and hazard mitigation tool at the MVO and may open several lines of research regarding dome failure mechanisms and pyroclastic flow propagation.

Acknowledgements

This study used data collected by the MVO on a network installed by the British Geological Survey (BGS). The MVO is a statutory body of the Government of Montserrat and is partially funded by the British Department of International Development. The technical and professional staff, including Venus Bass, Dave Williams, Carlisle 'Pyiko' Williams and Racquel 'Tappy' Syers, all with the MVO, provided field and laboratory support. Levar Cabey extracted some of the events used in this study. Paul and Elizabeth Breuer provided the photo of the February 25, 2001, pyroclastic flow. David Lea and Dave Williams dubbed a portion of MVO video for the August 12, 1999, event. Philippe Jousset and Jurgen Neuberg made several suggestions that improved this study. Marie Edmonds sampled the July 4, 2001, deposits and Maartin Felix suggested that the observed velocity increase for the August 12, 1999, event might be a result of channeled flow in the Tar River Valley. All are gratefully thanked. Steve McNutt and an anonymous reviewer provided useful comments that improved the manuscript. This research was partially funded by the European Union through a grant to MULTIMO. This paper is published with permission of the Director of the BGS and the Director of the MVO.

References

Aki, K., Ferrazzini, V., 2000. Seismic monitoring and modeling of an active volcano for prediction. J. Geophys. Res. 105, 16617–16640.

Aki, K., Koyanagi, R.Y., 1981. Deep volcanic tremor and magma ascent mechanism under Kilauea Hawaii. J. Geophys. Res. 86, 7095–7110.

Benoit, J., McNutt, S., 1997. New constraints on source processes of volcanic tremor at Arenal Volcano, Costa Rica, using broadband seismic data. Geophys. Res. Let. 24, 449–452.

Calder, E.S., Cole, P.D., Dade, W.B., Druitt, T.H., Hobblitt, R.P., Huppert, H.E., Ritchie, L., Sparks, R.S.J., Young, S.R., 1999. Mobility of pyroclastic flows and surges at Soufriere Hills Volcano, Montserrat. Geophys. Res. Lett. 26, 537–540.

Chouet, B.A., 1988. Resonance of a fluid-driven crack: Radiation properties and implications for the source of long-period events and harmonic tremor. J. Geophys. Res. 93, 4373–4400.

Fehler, M., 1983. Observations of volcanic tremor at Mount St. Helens Volcano. J. Geophys. Res. 88, 3476–3484.

Gottschammer, E., Surono, I., 2000. Locating tremor and shock sources recorded at Bromo Volcano. J. Volcan. Geoterm. Res. 101, 199–209.

Jolly, A.D., 2000. Subsurface structure of the volcanoes of Katmai National Park. Ph.D. Thesis, University of Alaska, Fairbanks, AK, 167 pp.

Lahr, J.C., 1989. HYPOELLIPSE/Version 2.0: A computer program for determining local earthquake hypocentral parameters, magnitude, and first motion pattern, U.S. Geol. Surv. Open File Rep. 89-23, 89 pp.

McNutt, S.R., Tytgat, G.C., Power, J.A., 1995. Preliminary analysis of tremor associated with the 1999 eruptions of Crater Peak, Mount Spurr Volcano, Alaska, in The 1992 eruptions of Crater Peak Vent, Mount Spurr volcano, Alaska. U.S. Geol. Surv. Bull. 2139, 161–177.

Miller, T.P., Chouet, B.A., 1994. An introduction and chro-

nology to the 1989–1990 eruption of Redoubt Volcano, Alaska. J. Volcan. Geotherm. Res. 62, 1–10.

Nakada, S., Shimizu, H., Ohta, K., 1999. Overview of the 1990–1995 eruption at Unzen Volcano. J. Volcan. Geotherm. Res. 89, 1–22.

Neuberg, J., Luckett, R., Baptie, B., Olsen, K., 2000. Models of tremor and low-frequency earthquake swarms. J. Volcan. Geotherm. Res. 101, 83–104.

Norton, G.E., Watts, R.B, Voight, B., Mattioli, G., Herd, R.A., Young, S.R., Devine, J., Aspinall, W.P., Bonadonna, C., Baptie, B.J., Edmonds, M., Harford, C.L., Jolly, A.D., Loughlin, S.C., Luckett, R., Sparks, R.S.J., in press, Pyroclastic flow and explosive activity at Soufrière Hills Volcano, Montserrat, during a period of virtually no magma extrusion (March 1998 to November 1999). In: Druitt, T.H., Kokelaar, B.P. (Eds.), The eruption of Soufrière Hills Volcano, Montserrat, from 1995 to 1999. Geol. Soc. London Mem.

Power, J.A., Wyss, M., Latchman, J.L., 1998. Spatial variations in the frequency-magnitude distribution of earthquakes at Soufriere Hills Volcano, Montserrat, West Indies. Geophys. Res. Lett. 25, 3653–3656.

Rowe, C.A., Aster, R.C., Kyle, P.R., Dibble, R.R., Schlue, J.W., 2000. Seismic and acoustic observations at Mt. Erebus Volcano, Ross Island, Antarctica, 1994–1998. J. Volcan. Geotherm. Res. 101, 105–128.

Uhira, K., Yamasato, H., Takeo, M., 1994. Source mechanism of seismic waves excited by pyroclastic flows observed at Unzen volcano, Japan. J. Geophys. Res. 99, 17757–17773.

Ui, T., Matsuwo, N., Sumita, M., Fujinawa, A., 1999. Generation of block and ash flows during the 1990–1995 eruption of Unzen Volcano, Japan.. J. Volcan. Geotherm. Res. 89, 123–137.

Voight, B., Sukhyar, R., Wirakusumah, A.D., 2000. Introduction to the special issue on Merapi Volcano. J. Volcan. Geotherm. Res. 100, 1–8.

Wiemer, S., McNutt, S.R., 1997. Variations in the frequency-magnitude distribution with depth in two volcanic areas: Mount St. Helens, Washington, and Mt. Spurr, Alaska. Geophys. Res. Lett. 24, 189–192.

Wu, H., Lees, J.M., 1996. Attenuation Structure of Coso Geothermal Area, California, from Wave Pulse Widths. Bull. Seismol. Soc. Am. 86, 1574–1590.

Yamasoto, H., 1997. Quantitative analysis of pyroclastic flows using infrasound and seismic data at Unzen, Japan. J. Phys. Earth 45, 297–416.

Young, S., Sparks, R.S.J., Aspinall, W., Lynch, L., Miller, A., Robertson, R.E.A., Shepherd, J.B., 1998. Overview of the eruption of Soufriere Hills volcano, Montserrat, 18 July, 1995 to December 1997. Geophys. Res. Lett. 25, 3389–3392.

Zucca, J.J., Evans, J.R., 1992. Active High-Resolution Compressional Wave Attenuation Tomography at Newberry Volcano, Central Cascade Range. J. Geophys. Res. 97, 11047–11055.